

A Convex Approximation for a PDE Constrained Fractional Optimization Problem with an Application to Photonic Crystal Design

Mengyue Wu¹, Jianhua Yuan^{1,*} and Jianxin Zhang¹

¹ School of Science, Beijing University of Post and Telecommunications, Beijing 100876, China

Received 5 January 2022; Accepted (in revised version) 20 June 2022

Abstract. Based on a subspace method and a linear approximation method, a convex algorithm is designed to solve a kind of non-convex PDE constrained fractional optimization problem in this paper. This PDE constrained problem is an infinite-dimensional Hermitian eigenvalue optimization problem with non-convex and low regularity. Usually, such a continuous optimization problem can be transformed into a large-scale discrete optimization problem by using the finite element methods. We use a subspace technique to reduce the scale of discrete problem, which is really effective to deal with the large-scale problem. To overcome the difficulties caused by the low regularity and non-convexity, we creatively introduce several new artificial variables to transform the non-convex problem into a convex linear semidefinite programming. By introducing linear approximation vectors, this linear semidefinite programming can be approximated by a very simple linear relaxation problem. Moreover, we theoretically prove this approximation. Our proposed algorithm is used to optimize the photonic band gaps of two-dimensional Gallium Arsenide-based photonic crystals as an application. The results of numerical examples show the effectiveness of our proposed algorithm, while they also provide several optimized photonic crystal structures with a desired wide-band-gap. In addition, our proposed algorithm provides a technical way for solving a kind of PDE constrained fractional optimization problems with a generalized eigenvalue constraint.

AMS subject classifications: 49M37, 65K10, 90C05, 90C06, 90C26

Key words: PDE constrained optimization, fractional programming, linear approximation, finite element method, photonic band gap.

*Corresponding author.

Email: jianhuayuan@bupt.edu.cn (J. Yuan)

1 Introduction

A PDE constrained optimization problem refers to the optimization of systems governed by partial differential equations (PDEs), which appear as constraints in the optimization problem [8]. In recent years, the PDE constrained optimization problem has become an important research field due to its wide application in engineering and other related fields, such as photonic crystal (PhC) structure design, liquid flow, flow control, weather forecasting, and so on [5, 6, 11, 24].

In this paper, we investigate a kind of PDE constrained optimization problem, which is in the study of the periodic band structure of micro-nanometer materials [7]. This problem can be written in the form of (1.1)

$$\begin{cases} \max_y J(y) = \frac{f(y)}{g(y)} \\ \text{s.t. } A(u(y)) = \lambda(y)B(u(y)), \end{cases} \quad (1.1)$$

where y is the variable, and $J(y)$ is the cost functional. $f(y)$, $g(y)$, $u(y)$ and $\lambda(y)$ are functions of y . The constraint equation of (1.1) is written as a generalized eigenvalue equation, with A and B being functionals caused by the actual constraint. The problem (1.1) is an infinite-dimensional and nonlinear optimization problem with a fractional objective. These bring great difficulties to the theoretical analysis and numerical solution of this non-convex PDE constraint problem.

The photonic band gaps (PBGs) optimization problem of PhC is such a PDE constrained optimization problem in the form of the problem (1.1). As an artificial material with a periodic structure, PhCs have PBGs that can prohibit electromagnetic waves (EMWs) from propagating in certain frequency regions [2, 14, 17]. The PBGs have a wide range of industrial applications such as microwave engineering, semiconductor, laser technology, and so on [9, 10, 20, 23]. When designing PhCs, the controllable frequency bands of EMWs, i.e., the bandgap should be as big as possible to meet the actual needs. Due to the lack of fundamental length scale in Maxwell's equations, it can be shown that the magnitude of the bandgap scales by a factor of s when the crystal is expanded by a factor of $1/s$. It is more meaningful to maximize the gap ratio instead of the absolute bandgap [17]. Therefore, the objective of the PBGs optimization problem in our work is the gap ratio which is a fractional function. The propagation of electromagnetic waves can finally be governed by generalized eigenvalue equations, which is a non-convex PDE constraint of the PBGs optimization problem.

There are many approaches to solve the PBGs optimization problem, such as level set methods and other gradient-based optimization methods with prescribed inclusion shapes, fixed topology, or geometric considerations [19, 21, 29, 30]. However, gradient-based solution methods often suffer from the lack of regularity of the underlying problem when eigenvalue multiplicities are present, as they are typically at or near the solution [24, 33]. The discretization of PDE is involved when a traditional optimization

method is used to solve the PBGs optimization problem. Examples of common discrete methods include: the finite element method (FEM), the finite difference method, the Galerkin spectral approximations, and the mixed finite element method [?, ?, 12, 18, 28, 36–39]. The FEM is usually used to discretize the continuous problem due to its higher calculation accuracy and advantages in solving problems posed on complex domains [15, 16, 32, 35]. For the problem (1.1), the constraint equations can be discretized by using the FEM. Then how to design an effective optimization algorithm is a challenge for solving the discrete system. In recent years, an algorithm combining a subspace method and convex optimization is used to solve PBGs optimization problems, which improves the calculation accuracy to a certain extent [24, 25]. This algorithm provides an idea to design a more simple and efficient algorithm for the PBGs optimization problem, which is the motivation of our work. We want to design a fast algorithm to solve the PBGs optimization problem and present the corresponding theoretical analysis.

In this paper, we design a new algorithm to solve the PBGs optimization problem, which is based on a finite element method, subspace method and linear approximation method. First, we use a FEM to transform the continuous optimization problem into a discrete optimization problem. This discrete problem is a large-scale non-convex low regularity problem with a fractional objective. To overcome these difficulties, a new approach combining the subspace method and linear approximation method is designed. The large number theorem is used to prove the effectiveness of the linear approximation method. The subspace methods have been proved to be an effective algorithm to reduce the scale of the discrete problem [4, 24, 26]. In our approach, the parameters of the subspace method are redesigned based on several small numerical tests to improve computational efficiency. We keep the subspaces fixed at a given decision parameter vector and use a reparametrization of the decision variables to obtain a semidefinite PBGs optimization problem. This semidefinite PBGs optimization problem is transformed into a convex linear SDP by introducing several new artificial variables. Then, via approximation of the semidefinite cones by judiciously chosen linear bases, a new linear programming (LP) formulation of the PBGs optimization is obtained. Although being a somewhat heuristic method, the LP relaxation has shown improved performance when solving the PBGs optimization problems. Furthermore, we theoretically prove that the LP relaxation problem can approximate the linear SDP problem.

To show the effectiveness of our proposed algorithm, the optimal structures of Gallium Arsenide (GaAs)-based PhC are designed. The existing results have shown that the GaAs-based PhC improved the optical performance of one-dimensional PhCs devices significantly [3, 13]. A two-dimensional GaAs-based PhC may also improve the optical properties of PhCs devices. We use our algorithm to optimize two-dimensional GaAs-based PhCs with square lattice and hexagonal lattice respectively. The optimized results demonstrate the superiority of our algorithm. The calculation time is reduced after the semidefinite PBGs optimization problem is transformed into the LP form. The optimized structures of PhCs with wide-band-gap provide the possibility for the fabrication of PhCs. Our works not only design an efficient algorithm for the optimization

problem proposed in this paper, but also provide a new technical way for solving PDE constrained fractional optimization problems with generalized eigenvalue constraints. In addition, our works provide the mathematical model, numerical algorithm and simulation guidance for the fabrication of PhCs.

2 A generalized eigenvalue constrained optimization problem

Given a medium distribution, we can calculate the band structure of the material. The common crystal systems of two-dimensional PhCs include square lattice and hexagonal lattice (inside), and their PhC structure and band structure are shown in Fig. 1 and Fig. 2 respectively. The gaps are also shown in these two figures. In the structure design of PhCs, we focus on which periodic structure of two materials can produce the largest PBG around a particular frequency, i.e., maximize m -th gap ratio.

The objective of PBGs optimization problem that maximizes the gap ratio between λ^m and λ^{m+1} is defined as [24]

$$\max_{\varepsilon} J(\varepsilon(\mathbf{r})) = \frac{\inf_{\mathbf{k} \in \partial\mathcal{B}} \lambda^{m+1}(\varepsilon, \mathbf{k}) - \sup_{\mathbf{k} \in \partial\mathcal{B}} \lambda^m(\varepsilon, \mathbf{k})}{\inf_{\mathbf{k} \in \partial\mathcal{B}} \lambda^{m+1}(\varepsilon, \mathbf{k}) + \sup_{\mathbf{k} \in \partial\mathcal{B}} \lambda^m(\varepsilon, \mathbf{k})}, \quad (2.1)$$

where $\partial\mathcal{B}$ represents the irreducible Brillouin zone boundary as shown on the right of Fig. 3 and Fig. 4, and \mathbf{k} is a wave vector in $\partial\mathcal{B}$. As we mentioned in Section 1, the constraint of the PBGs optimization problem is a generalized eigenvalue equation. And note λ^m as the m -th eigenvalue of the generalized eigenvalue equation, assume that these eigenpairs are numbered in ascending order: $0 \leq \lambda^1 \leq \lambda^2 \leq \dots \leq \lambda^\infty$.

Now, we present the specific process of transforming Maxwell's equations into a generalized eigenvalues equation. For general time dependent electromagnetic fields,

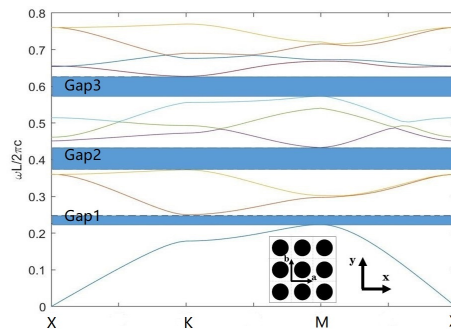


Figure 1: A initial PhC structure with square lattice (inset) and its band structure.

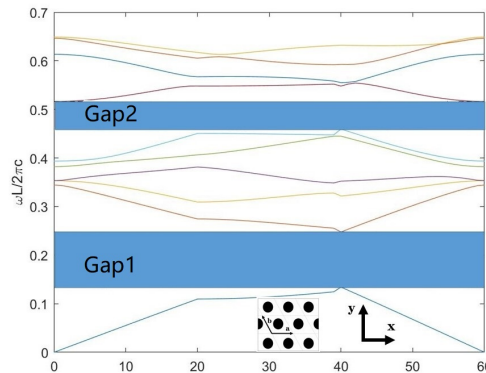


Figure 2: A initial PhC structure with hexagonal lattice (inset) and its band structure.

Maxwell’s equations in the differential form are given by [1]

$$\nabla \times \mathbf{E} = -\frac{\partial \mathbf{B}}{\partial t}, \quad \nabla \times \mathbf{H} = \frac{\partial \mathbf{D}}{\partial t} + \mathbf{J}, \quad \nabla \cdot \mathbf{D} = \rho, \quad \nabla \cdot \mathbf{B} = 0,$$

where \mathbf{E} is the electric field intensity, \mathbf{D} is the electric flux density, \mathbf{H} is magnetic field intensity, \mathbf{B} is magnetic flux density, \mathbf{J} is the electric current density, and ρ is electric charge density.

Consider that the field is a time-harmonic field, the medium is linear and isotropic, the magnetic permeability is constant and in the absence of sources with a monochromatic wave. \mathbf{E} and \mathbf{H} can be written as follows:

$$\mathbf{H}(\mathbf{r}, t) = \mathbf{H}(\mathbf{r})e^{-i\omega t} \quad \text{and} \quad \mathbf{E}(\mathbf{r}, t) = \mathbf{E}(\mathbf{r})e^{-i\omega t},$$

then Maxwell’s equations can be written in the following form:

$$\begin{aligned} \nabla \times \left(\frac{1}{\varepsilon(\mathbf{r})} \nabla \times \mathbf{H}(\mathbf{r}) \right) &= \left(\frac{\omega}{c} \right)^2 \mathbf{H}(\mathbf{r}) && \text{in } \mathbb{R}^3, \\ \frac{1}{\varepsilon(\mathbf{r})} \nabla \times (\nabla \times \mathbf{E}(\mathbf{r})) &= \left(\frac{\omega}{c} \right)^2 \mathbf{E}(\mathbf{r}) && \text{in } \mathbb{R}^3, \end{aligned}$$

where $\varepsilon(\mathbf{r})$ is the dielectric function and c is the speed of light.

In transverse electric field (TE), the electric field is in the $x - y$ plane and the magnetic field $\mathbf{H}(\mathbf{r}) = (0, 0, H(\mathbf{r}))$ is perpendicular to this plane. In transverse magnetic field (TM), the magnetic field is in the $x - y$ plane and the electric field $\mathbf{E}(\mathbf{r}) = (0, 0, E(\mathbf{r}))$ is perpendicular to this plane. Thus, the equations become

$$\text{TE:} \quad -\nabla \cdot \left(\frac{1}{\varepsilon(\mathbf{r})} \nabla H(\mathbf{r}) \right) = \left(\frac{\omega}{c} \right)^2 H(\mathbf{r}) \quad \text{in } \mathbb{R}^2, \tag{2.2a}$$

$$\text{TM:} \quad -\nabla \cdot (\nabla E(\mathbf{r})) = \left(\frac{\omega}{c} \right)^2 \varepsilon(\mathbf{r}) E(\mathbf{r}) \quad \text{in } \mathbb{R}^2. \tag{2.2b}$$

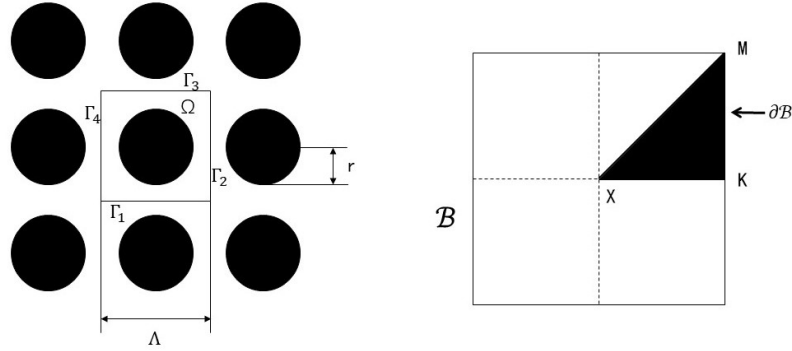


Figure 3: Left: a cross section of a square lattice. The box represents the primitive unit cell Ω , Λ is the periodicity length of the lattice, r is the radius of dielectric, and $\Gamma_i, i=1, \dots, 4$ is the boundary of Ω . Right: the first Brillouin zone B . The irreducible zone is the black triangular wedge, and its boundary is denoted by ∂B .

For two-dimensional square lattices and hexagonal lattices, the dielectric function satisfies $\varepsilon(\mathbf{r}) = \varepsilon(\mathbf{r} + \mathbf{R})$, where \mathbf{R} are the crystal lattice vectors. \mathbf{R} denote the vectors spanned by $\{\Lambda \mathbf{e}_x, \Lambda \mathbf{e}_y\}$, where \mathbf{e}_x and \mathbf{e}_y are the unit basis vectors and Λ is the periodicity length of the crystal.

By applying the Bloch-Floquet theory for periodic eigenvalue problems, we obtain that

$$H(\mathbf{r}) = e^{i\mathbf{k} \cdot \mathbf{r}} H_{\mathbf{k}}(\mathbf{r}) \quad \text{and} \quad E(\mathbf{r}) = e^{i\mathbf{k} \cdot \mathbf{r}} E_{\mathbf{k}}(\mathbf{r}). \tag{2.3}$$

$H_{\mathbf{k}}(\mathbf{r})$ and $E_{\mathbf{k}}(\mathbf{r})$ are periodic solutions such that $H(\mathbf{r})$ and $E(\mathbf{r})$ are quasi-periodic functions. This means

$$\begin{aligned} H_{\mathbf{k}}(\mathbf{r})|_{\Gamma_1} &= H_{\mathbf{k}}(\mathbf{r})|_{\Gamma_3}, & H_{\mathbf{k}}(\mathbf{r})|_{\Gamma_2} &= H_{\mathbf{k}}(\mathbf{r})|_{\Gamma_4}, \\ E_{\mathbf{k}}(\mathbf{r})|_{\Gamma_1} &= E_{\mathbf{k}}(\mathbf{r})|_{\Gamma_3}, & E_{\mathbf{k}}(\mathbf{r})|_{\Gamma_2} &= E_{\mathbf{k}}(\mathbf{r})|_{\Gamma_4}, \end{aligned}$$

and the $\Gamma_i, i=1, \dots, 4$, are boundaries of a unit cell Ω as shown in Fig. 3 and Fig. 4.

Then substitute (2.3) into (2.2a) and (2.2b) respectively, we can get:

$$\text{TE:} \quad -(\nabla + i\mathbf{k}) \cdot \left(\frac{1}{\varepsilon(\mathbf{r})} (\nabla + i\mathbf{k}) H_{\mathbf{k}}(\mathbf{r}) \right) = \left(\frac{\omega}{c} \right)^2 H_{\mathbf{k}}(\mathbf{r}) \quad \text{in } \Omega, \tag{2.4}$$

$$\text{TM:} \quad -(\nabla + i\mathbf{k}) \cdot ((\nabla + i\mathbf{k}) E_{\mathbf{k}}(\mathbf{r})) = \left(\frac{\omega}{c} \right)^2 \varepsilon(\mathbf{r}) E_{\mathbf{k}}(\mathbf{r}) \quad \text{in } \Omega. \tag{2.5}$$

For notational convenience, note that $\lambda = \omega^2/c^2$. The above equations (2.4) and (2.5) can be written in the following operator form:

$$-(\nabla + i\mathbf{k}) \cdot [\rho(\nabla + i\mathbf{k})u] = \lambda \kappa u \quad \text{in } \Omega, \tag{2.6}$$

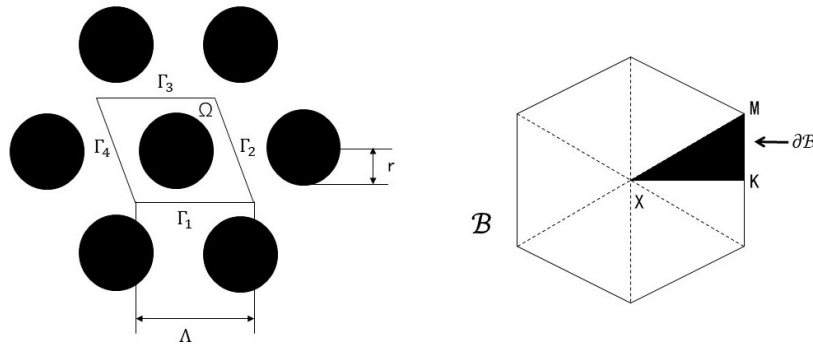


Figure 4: Left: a cross section of a hexagonal lattice. The box represents the primitive unit cell Ω , Λ is the periodicity length of the lattice, r is the radius of dielectric, and $\Gamma_i, i=1, \dots, 4$ is the boundary of Ω . Right: the first Brillouin zone \mathcal{B} . The irreducible zone is the black triangular wedge, and its boundary is denoted by $\partial\mathcal{B}$.

where

$$u = \begin{cases} E_{\mathbf{k}}(\mathbf{r}) & \text{in TM case,} \\ H_{\mathbf{k}}(\mathbf{r}) & \text{in TE case,} \end{cases} \quad \rho = \begin{cases} 1 & \text{in TM case,} \\ \frac{1}{\varepsilon(\mathbf{r})} & \text{in TE case,} \end{cases}$$

$$\kappa = \begin{cases} \varepsilon(\mathbf{r}) & \text{in TM case,} \\ 1 & \text{in TE case.} \end{cases}$$

And we denote the m -th pair of eigenfunction and eigenvalue of (2.6) by (u^m, λ^m) .

With the periodic boundary condition, the PBGs optimization problem can be written as:

$$\begin{cases} \max_{\varepsilon} J(\varepsilon(\mathbf{r})) = \frac{\inf_{\mathbf{k} \in \partial\mathcal{B}} \lambda^{m+1}(\varepsilon, \mathbf{k}) - \sup_{\mathbf{k} \in \partial\mathcal{B}} \lambda^m(\varepsilon, \mathbf{k})}{\inf_{\mathbf{k} \in \partial\mathcal{B}} \lambda^{m+1}(\varepsilon, \mathbf{k}) + \sup_{\mathbf{k} \in \partial\mathcal{B}} \lambda^m(\varepsilon, \mathbf{k})} & (2.7) \\ \text{s.t. } -(\nabla + i\mathbf{k}) \cdot [\rho(\nabla + i\mathbf{k})u] = \lambda\kappa u & \text{in } \Omega, \\ u|_{\Gamma_1} = u|_{\Gamma_3}, \quad u|_{\Gamma_2} = u|_{\Gamma_4} & \text{on } \Gamma = \cup_{i=1}^4 \Gamma_i. \end{cases}$$

3 Variational formulation and finite element discretization

According to the discussion in Section 2, the electromagnetic propagation law in PhCs can be described by the following system: for given $\mathbf{k} \in \partial\mathcal{B}$, find u and λ satisfy

$$\begin{cases} -(\nabla + i\mathbf{k}) \cdot [\rho(\nabla + i\mathbf{k})u] = \lambda\kappa u & \text{in } \Omega, \\ u|_{\Gamma_1} = u|_{\Gamma_3}, \quad u|_{\Gamma_2} = u|_{\Gamma_4} & \text{on } \Gamma = \cup_{i=1}^4 \Gamma_i, \end{cases} \quad (3.1)$$

where

$$\rho = \begin{cases} 1 & \text{in TM case,} \\ \frac{1}{\varepsilon(\mathbf{r})} & \text{in TE case,} \end{cases} \quad \kappa = \begin{cases} \varepsilon(\mathbf{r})I & \text{in TM case,} \\ I & \text{in TE case.} \end{cases}$$

Here we first define a Sobolev space

$$\mathbb{V} = \{v | v \in H^1(\Omega), v|_{\Gamma_1} = v|_{\Gamma_3}, v|_{\Gamma_2} = v|_{\Gamma_4}\}.$$

Using the Galerkin variational principle, (3.1) can be rewritten as: For given $\mathbf{k} \in \partial\mathcal{B}$, find $u \in \mathbb{V}$ and $\lambda \in \mathbb{R}$ such that

$$\langle \rho(\nabla + i\mathbf{k})u, (\nabla + i\mathbf{k})v \rangle = \langle \lambda \kappa u, v \rangle, \quad \forall v \in \mathbb{V}, \tag{3.2}$$

where $\langle \cdot, \cdot \rangle$ represents the standard inner product of $L^2(\Omega)$.

It is easy to know that the bilinear form $\langle \rho(\nabla + i\mathbf{k})u, (\nabla + i\mathbf{k})v \rangle$ is a bounded functional in the space \mathbb{V} , and according to the classical theory of eigenvalues [22], it is known that the solution of the variational problem (3.2) exists.

Next, we discretize the bilinear form (3.2) by using a FEM. The unit cell Ω is divided into a finite number of n -simplex subcells denoted by T . We consider a family of triangulations $\{T_h\}$ consist of n -simplex T which satisfy

$$\bar{\Omega} = \sum_{T \in T_h} T$$

and suppose all the triangulations used in this work are shape regular. For $T \in T_h$, h_T denotes the maximal diameter of each n -simplex T and $h = \max_{T \in T_h} h_T$. Let \mathcal{P} denote the set of vertices of the triangulation. And let N denote the number of subcells and L be the number of vertices.

A typical characterization of the dielectric function $\varepsilon(\mathbf{r})$ is the distribution of two distinct materials. Suppose that we are given two different materials with dielectric constants ε_{\min} and ε_{\max} , and $\varepsilon_{\min} \leq \varepsilon_{\max}$. Our dielectric function $\varepsilon(\mathbf{r})$ takes a unique value between ε_{\min} and ε_{\max} on each subcell. And the dielectric function $\varepsilon(\mathbf{r})$ is discretized into a finite-dimensional vector $\varepsilon = (\varepsilon_1, \varepsilon_2, \dots, \varepsilon_N)$. Moreover, to render this problem computationally tractable, we replace the irreducible Brillouin zone boundary $\partial\mathcal{B}$ with a finite subset

$$\mathcal{S} = \{\mathbf{k}_t | \mathbf{k}_t \in \partial\mathcal{B}, 1 \leq t \leq n_k\},$$

where $\mathbf{k}_t, 1 \leq t \leq n_k$, are wave vectors chosen along the irreducible Brillouin zone boundary.

Define the following finite dimensional subspaces:

$$\mathbb{V}_h = \{v_h \in H^1(\Omega) | v_h|_T \in P_1, v_h|_{\Gamma_1} = v_h|_{\Gamma_3}, v_h|_{\Gamma_2} = v_h|_{\Gamma_4}, \forall T \in T_h\},$$

where P_1 is the space of polynomials of degree less than or equal to 1.

Thus, the finite element discretizations of (3.2) are given by the following: For given $\mathbf{k} \in \mathcal{S}$, find $u_h \in \mathbb{V}_h$ and $\lambda_h \in \mathbb{R}$ such that

$$\langle \rho(\nabla + i\mathbf{k})u_h, (\nabla + i\mathbf{k})v_h \rangle - \langle \lambda_h \kappa u_h, v_h \rangle = 0, \quad \forall v_h \in \mathbb{V}_h. \tag{3.3}$$

Let $\phi_i(x, y), i = 1, \dots, L$, be the basis functions corresponding to the point x_i . And we can define

$$u_h = \sum_{i=1}^L u_i \phi_i(x, y),$$

where $u_i = u_h(x_i)$ for $x_i \in \mathcal{P}$.

Define

$$\mathbf{R} = (\phi_1(x, y), \phi_2(x, y), \dots, \phi_L(x, y)) \quad \text{and} \quad \mathbf{u}_h = (u_h^1, u_h^2, \dots, u_h^L)^T.$$

Obviously, we can get that $u_h = \mathbf{R}\mathbf{u}_h$. Then, the finite element discretization for the state constraints can be rewritten in the following form:

$$A_h(\varepsilon, \mathbf{k})\mathbf{u}_h = \lambda_h B_h(\varepsilon)\mathbf{u}_h, \quad \mathbf{k} \in \mathcal{S}.$$

The matrices A_h are B_h are given by:

$$A_h = [\langle \rho_j(\nabla + i\mathbf{k})\phi_j, (\nabla + i\mathbf{k})\phi_i \rangle] \in \mathbb{C}^{L \times L},$$

$$B_h = [\langle \kappa_j \phi_j, \phi_i \rangle] \in \mathbb{R}^{L \times L}.$$

These matrices are sparse and typically very large. And, we consider the approximate eigenvalues in ascending order: $\lambda_h^1 \leq \lambda_h^2 \leq \dots \leq \lambda_h^L$.

Now, we can express the finite element approximation of the PBGs optimization problem (M_1) as

$$(M_1): \begin{cases} \max_{\varepsilon} J(\varepsilon(\mathbf{r})) = \frac{\min_{\mathbf{k} \in \mathcal{S}} \lambda_h^{m+1}(\varepsilon, \mathbf{k}) - \max_{\mathbf{k} \in \mathcal{S}} \lambda_h^m(\varepsilon, \mathbf{k})}{\min_{\mathbf{k} \in \mathcal{S}} \lambda_h^{m+1}(\varepsilon, \mathbf{k}) + \max_{\mathbf{k} \in \mathcal{S}} \lambda_h^m(\varepsilon, \mathbf{k})} \\ \text{s.t. } A_h(\varepsilon, \mathbf{k})u_h^j = \lambda_h^j B_h(\varepsilon)u_h^j, & j = m, m+1, \quad \forall \mathbf{k} \in \mathcal{S}, \\ \varepsilon_{\min} \leq \varepsilon_i \leq \varepsilon_{\max}, & 1 \leq i \leq N. \end{cases} \tag{3.4}$$

Here, $A_h(\varepsilon, \mathbf{k}) \in \mathbb{C}^{N \times N}$ is a Hermitian stiffness matrix and $B_h(\varepsilon) \in \mathbb{R}^{N \times N}$ is a symmetric positive definite mass matrix. The matrices A_h and B_h can be written as the sum of augmented stiffness matrices on each element. For the convenience of subsequent calculations, they are recorded in the following form. In TE case,

$$A_h = \sum_{i=1}^N \frac{1}{\varepsilon_i} A_{h,i}^{TE}$$

depends on $\varepsilon = (\varepsilon_1, \varepsilon_2, \dots, \varepsilon_N)$ while B_h does not. In TM case,

$$B_h = \sum_{i=1}^N \varepsilon_i B_{h,i}^{TM}$$

depends on $\varepsilon = (\varepsilon_1, \varepsilon_2, \dots, \varepsilon_N)$ while A_h does not.

Unfortunately, with a fractional objective, this problem is large-scale non-convex and low regularity. There are no existing algorithms that can directly solve such a complex optimization problem.

4 Optimal algorithm

In this section, we design a new algorithm based on a new subspace method to reduce the scale of the problem (M_1). Further, a convex optimization technique is used to transform the non-convex problem into a linear programming problem.

4.1 A new subspace method

The PBGs optimization problem (M_1) is a large-scale problem after the FEM discretization. In order to improve the computational efficiency, we first consider a subspace method to reduce the size of problem (M_1).

Let $\hat{\varepsilon}$ be the current iterate. We construct two subspace matrices for each of the target bandgaps at each $\mathbf{k} \in \partial\mathcal{B}$. For each $\mathbf{k} \in \partial\mathcal{B}$, we have

$$\Phi_l^{\hat{\varepsilon}} = [u_h^{m-a_k+1}(\hat{\varepsilon}, \mathbf{k}), \dots, u_h^m(\hat{\varepsilon}, \mathbf{k})] \quad \text{and} \quad \Phi_u^{\hat{\varepsilon}} = [u_h^{m+1}(\hat{\varepsilon}, \mathbf{k}), \dots, u_h^{m+b_k}(\hat{\varepsilon}, \mathbf{k})],$$

where $u_h^i(\hat{\varepsilon}, \mathbf{k})$ are the orthonormal eigenvectors of the Hermitian eigenvalue equation, the constraint of problem (M_1), with $\varepsilon = \hat{\varepsilon}$. Ideally, $\Phi_l^{\hat{\varepsilon}}$ and $\Phi_u^{\hat{\varepsilon}}$ should include all the lower m eigenvectors and all the higher $N - m$ eigenvectors, respectively. But the numerical simulations would be too expensive under the circumstances. In this paper, we use a small important subset of these eigenvectors to reduce the computation cost. A new subspace method is designed to determine the parameters a_k, b_k . The specific form is as follows:

$$a_k = \min\{7, m\}, \quad b_k = \min\{7, N - m\}.$$

We did many small numerical simulations to determine the parameters of the subspace method to improve the computational efficiency. Numerous numerical experiments have shown that the number 7 can maximize the efficiency of the calculation while maintaining the accuracy of the calculation.

Define two additional decision variables:

$$\lambda_h^u = \min_{\mathbf{k} \in \partial\mathcal{B}} \lambda_h^{m+1}(\varepsilon, \mathbf{k}) \quad \text{and} \quad \lambda_h^l = \max_{\mathbf{k} \in \partial\mathcal{B}} \lambda_h^m(\varepsilon, \mathbf{k}). \quad (4.1)$$

Then the problem (M_1) can be rewritten as follows:

$$\left\{ \begin{array}{l} \max_{\varepsilon} \quad J(\varepsilon(\mathbf{r})) = \frac{\lambda_h^u - \lambda_h^l}{\lambda_h^u + \lambda_h^l} \\ \text{s.t.} \quad \Phi_l^{\hat{\varepsilon}^*}(\mathbf{k}) [A_h(\varepsilon, \mathbf{k}) - \lambda_h^l B_h(\varepsilon)] \Phi_l^{\hat{\varepsilon}}(\mathbf{k}) \leq 0, \quad \forall \mathbf{k} \in \mathcal{S}, \\ \quad \quad \Phi_u^{\hat{\varepsilon}^*}(\mathbf{k}) [A_h(\varepsilon, \mathbf{k}) - \lambda_h^u B_h(\varepsilon)] \Phi_u^{\hat{\varepsilon}}(\mathbf{k}) \geq 0, \quad \forall \mathbf{k} \in \mathcal{S}, \\ \quad \quad \varepsilon_{\min} \leq \varepsilon_i \leq \varepsilon_{\max}, \quad i = 1, \dots, N, \\ \quad \quad \lambda_h^l, \lambda_h^u \geq 0. \end{array} \right. \tag{4.2}$$

The scale of problem (4.2) is much smaller than that obtained by the full subspaces, and this problem can be easily reformulated as linear semidefinite programming. Keeping subspaces fixed at $\hat{\varepsilon}$ can reduce the nonlinearity of the underlying problem.

4.2 Linear SDP form of the problem (M_1)

In order to simplify the problem and improve the computational efficiency, we first transform the problem (4.2) into linear SDP. The problem (4.2) can be rewritten as:

$$\left\{ \begin{array}{l} \max_y \quad \frac{\lambda_h^u - \lambda_h^l}{\lambda_h^u + \lambda_h^l} \\ \text{s.t.} \quad \Phi_l^{\hat{\varepsilon}^*}(\mathbf{k}) \left[\sum_{i=1}^N y_i M_i(\mathbf{k}) + y_{N+1} M_{N+1}(\mathbf{k}) \right] \Phi_l^{\hat{\varepsilon}}(\mathbf{k}) \leq 0, \quad \forall \mathbf{k} \in \mathcal{S}, \\ \quad \quad \Phi_u^{\hat{\varepsilon}^*}(\mathbf{k}) \left[\sum_{i=1}^N y_i M_i(\mathbf{k}) + y_{N+2} M_{N+2}(\mathbf{k}) \right] \Phi_u^{\hat{\varepsilon}}(\mathbf{k}) \geq 0, \quad \forall \mathbf{k} \in \mathcal{S}, \\ \quad \quad \varepsilon_{\min} \leq \varepsilon_i \leq \varepsilon_{\max}, \quad i = 1, \dots, N, \\ \quad \quad \lambda_h^l, \lambda_h^u \geq 0. \end{array} \right. \tag{4.3}$$

In TM case,

$$\mathbf{y} := (y_1, y_2, \dots, y_N, y_{N+1}, y_{N+2}) = \left(\varepsilon_1, \varepsilon_2, \dots, \varepsilon_N, \frac{1}{\lambda_h^l}, \frac{1}{\lambda_h^u} \right),$$

$M_i = -B_{h,i}^{TM}$, $i = 1, \dots, N$, and $M_{N+1} = M_{N+2} = A_h^{TM}(\mathbf{k})$. In TE case,

$$\mathbf{y} := (y_1, y_2, \dots, y_N, y_{N+1}, y_{N+2}) = \left(\frac{1}{\varepsilon_1}, \frac{1}{\varepsilon_2}, \dots, \frac{1}{\varepsilon_N}, \lambda_h^l, \lambda_h^u \right),$$

$M_i = A_{h,i}^{TE}(\mathbf{k})$, $i = 1, \dots, N$, and $M_{N+1} = M_{N+2} = -B_h^{TE}$.

Now, introduce the following new decision variable notation

$$\mathbf{z} := (z_1, z_2, \dots, z_N, z_{N+1}, z_{N+2}, z_{N+3}) = (sy_1, sy_2, \dots, sy_N, sy_{N+1}, sy_{N+2}, s),$$

where

$$s = \begin{cases} \left(\frac{1}{\lambda_h^l} + \frac{1}{\lambda_h^u}\right)^{-1} & \text{in TM case,} \\ \frac{1}{\lambda_h^l + \lambda_h^u} & \text{in TE case.} \end{cases}$$

The problem (4.3) can be equivalently translated into the following linear SDP:

$$\left\{ \begin{array}{l} \max_{\mathbf{z}} (-1)^d z_{N+1} + (-1)^{d+1} z_{N+2} \\ \text{s.t. } \Phi_l^{\hat{\epsilon}^*}(\mathbf{k}) \left[\sum_{i=1}^N z_i M_i(\mathbf{k}) + z_{N+1} M_{N+1}(\mathbf{k}) \right] \Phi_l^{\hat{\epsilon}}(\mathbf{k}) \preceq 0, \quad \forall \mathbf{k} \in \mathcal{S}, \\ \Phi_u^{\hat{\epsilon}^*}(\mathbf{k}) \left[\sum_{i=1}^N z_i M_i(\mathbf{k}) + z_{N+2} M_{N+2}(\mathbf{k}) \right] \Phi_u^{\hat{\epsilon}}(\mathbf{k}) \succeq 0, \quad \forall \mathbf{k} \in \mathcal{S}, \\ z_i + h_1 z_{N+3} \geq 0, \quad i = 1, \dots, N, \\ z_i + h_2 z_{N+3} \leq 0, \quad i = 1, \dots, N, \\ z_{N+1} + z_{N+2} = 1, \\ z_{N+1}, z_{N+2}, z_{N+3} \geq 0, \end{array} \right. \quad (4.4)$$

where

$$d = \begin{cases} 2 & \text{in TM case,} \\ 1 & \text{in TE case,} \end{cases} \quad h_1 = \begin{cases} -\epsilon_{\min} & \text{in TM case,} \\ -\frac{1}{\epsilon_{\max}} & \text{in TE case,} \end{cases}$$

$$h_2 = \begin{cases} -\epsilon_{\max} & \text{in TM case,} \\ -\frac{1}{\epsilon_{\min}} & \text{in TE case.} \end{cases}$$

The problem (4.4) is a simple convex linear SDP, and this problem can be efficiently solved by using an interior point method [34].

4.3 Linear programming

4.3.1 LP form of the problem (M_1)

From the definition of a positive semidefinite matrix, we know that a matrix H is positive semidefinite if and only if $v^T H v \geq 0$ for all non-zero vectors v . That is, a linear matrix inequality of the form

$$H(x)_{w \times w} = H_0 + \sum_{i=1}^n H_i x_i \succeq 0$$

is equivalent to

$$v^T H(x)v \geq 0, \quad \forall v \in \mathbb{R}^w.$$

Then, we approximate the above inequality by generating a finite number of approximating vectors $v_1, v_2, \dots, v_{N\nu} \in \mathbb{R}^w$. The method for choosing and updating these sets of vectors will be discussed in the next subsection. We can multiply the two linearized SDP constraints in (4.4) with appropriate approximating vectors, and obtain the following two linear inequalities:

$$\sum_{i=1}^N \Psi_{i,j}^1(\mathbf{k})z_i + \Psi_{N+1,j}^1(\mathbf{k})z_{N+1} \leq 0, \quad \forall \mathbf{k} \in \mathcal{S}, \quad j = 1, \dots, N\nu, \quad (4.5a)$$

$$\sum_{i=1}^N \Psi_{i,j}^2(\mathbf{k})z_i + \Psi_{N+2,j}^2(\mathbf{k})z_{N+2} \geq 0, \quad \forall \mathbf{k} \in \mathcal{S}, \quad j = 1, \dots, N\nu, \quad (4.5b)$$

where

$$\Psi_{i,j}^1(\mathbf{k}) = v_j^T \Phi_i^{\hat{\epsilon}^*}(\mathbf{k}) M_i(\mathbf{k}) \Phi_i^{\hat{\epsilon}}(\mathbf{k}) v_j \in \mathbb{R},$$

$$\Psi_{i,j}^2(\mathbf{k}) = v_j^T \Phi_u^{\hat{\epsilon}^*}(\mathbf{k}) M_i(\mathbf{k}) \Phi_u^{\hat{\epsilon}}(\mathbf{k}) v_j \in \mathbb{R}.$$

Replacing the semidefinite constraints in the problem (4.4) with their linear inequalities (4.5) and (4.6), we obtain the following linear programming problem (M_2):

$$(M_2): \begin{cases} \max_z (-1)^d z_{N+1} + (-1)^{d+1} z_{N+2} \\ \text{s.t.} \sum_{i=1}^N \Psi_{i,j}^1(\mathbf{k})z_i + \Psi_{N+1,j}^1(\mathbf{k})z_{N+1} \leq 0, \quad \forall \mathbf{k} \in \mathcal{S}, \quad j = 1, \dots, N\nu, \\ \sum_{i=1}^N \Psi_{i,j}^2(\mathbf{k})z_i + \Psi_{N+2,j}^2(\mathbf{k})z_{N+2} \geq 0, \quad \forall \mathbf{k} \in \mathcal{S}, \quad j = 1, \dots, N\nu, \\ z_i + h_1 z_{N+3} \geq 0, \quad i = 1, \dots, N, \\ z_i + h_2 z_{N+3} \leq 0, \quad i = 1, \dots, N, \\ z_{N+1} + z_{N+2} = 1, \\ z_{N+1}, z_{N+2}, z_{N+3} \geq 0. \end{cases}$$

4.3.2 Constructing the approximating vectors

Now, we describe our approach for constructing the approximating vectors $v_1, v_2, \dots, v_{N\nu} \in \mathbb{R}^w$. Ideally, the approximating vectors should be uniformly distributed over w -dimensional half-spherical surface:

$$HS^w = \left\{ v = (v^1, \dots, v^w)^T \in \mathbb{R}^w : \|v\|_2 = 1, v^w \geq 0 \right\}.$$

We only need to consider a half-sphere because

$$v^T \Psi v = (-v)^T \Psi (-v)$$

for any $v \in \mathbb{R}^w$, $\Psi \in \mathbb{R}^{w \times w}$. When N_v is big enough, vectors $v_1, v_2, \dots, v_{N_v} \in HS^w$ that follow a uniform distribution can approximate the half spherical surface.

Theorem 4.1. *Suppose the matrix $\Psi \in \mathbb{R}^{w \times w}$ is symmetric, and $v_k \in HS^w$, ($k = 1, 2, 3, \dots$) are samples that uniformly distributed over HS^w . Then, when $v_k^T \Psi v_k \geq 0$, ($k = 1, 2, 3, \dots$), the matrix Ψ is positive semidefinite.*

Proof. We know that the square of w -dimensional half-spherical surface is $\frac{\pi^{\frac{w}{2}}}{\Gamma(\frac{w}{2})}$, where $\Gamma(\cdot)$ is Gamma function. Define that

$$\Omega_{\Psi} = \left\{ v \in HS^w : v^T \Psi v < 0 \right\}.$$

Now, let's prove this theorem by contradiction. Suppose that matrix Ψ has negative eigenvalues. Then we know that the square of the set Ω_{Ψ} must be greater than 0, which is written as $S_{\Omega_{\Psi}}$. For any vector $v \in HS^w$ which is uniformly distributed over HS^w , the probability $P(v^T \Psi v < 0)$ of v satisfying $v^T \Psi v < 0$ is calculated as follows:

$$q := P(v^T \Psi v < 0) = S_{\Omega_{\Psi}} \left(\frac{\pi^{\frac{w}{2}}}{\Gamma(\frac{w}{2})} \right)^{-1} > 0.$$

Since $v_k^T \Psi v_k \geq 0$, ($k = 1, 2, 3, \dots$), we have $\mu_N \equiv 0$, ($N = 1, 2, 3, \dots$). μ_N is the number of samples who satisfy $v_k^T \Psi v_k < 0$ in the first N samples v_k , ($k = 1, \dots, N$).

According to Bernoulli's law of Large numbers, we have

$$\lim_{N \rightarrow +\infty} P\left(\left|\frac{\mu_N}{N} - q\right| < \epsilon\right) = \lim_{N \rightarrow +\infty} P\left(\left|\frac{0}{N} - q\right| < \epsilon\right) = 1, \quad \forall \epsilon > 0.$$

This means $P(q < \epsilon) = 1, \forall \epsilon > 0$. Then $q = 0$, which contradicts $q > 0$. Thus, the assumption that matrix Ψ has negative eigenvalues is invalid. That means the matrix Ψ is positive semidefinite. \square

Remark 4.1. In the numerical simulation, when the number of samples v_k is large enough, we can consider the matrix Ψ is positive semidefinite. And these vectors can be generated directly by using commercial softwares.

4.4 Main algorithm

We summarize our numerical approach for solving the PBGs optimization problem in the following Algorithm 4.1.

Algorithm 4.1 Implementation steps.

- 1: Confirm to optimize the m -th PBG, input an initial value \mathbf{z}^0 , and an error tolerance ϵ_{tol} . Set $\hat{\mathbf{z}} := \mathbf{z}^0$.
- 2: For each wave vector $\mathbf{k} \in S_{n_k}$, assemble the corresponding stiffness matrices A_h and B_h . And solve the generalized eigenvalue problem $A_h \mathbf{u}_h = \lambda_h B_h \mathbf{u}_h$.
- 3: Determine the subspace dimensions $a_k = \min\{7, m\}$ and $b_k = \min\{7, N - m\}$, and compute the matrices $\Phi_l^{\hat{\epsilon}}(\mathbf{k}) = [u_h^{m-a_k+1}(\hat{\epsilon}, \mathbf{k}), \dots, u_h^m(\hat{\epsilon}, \mathbf{k})]$ and $\Phi_u^{\hat{\epsilon}}(\mathbf{k}) = [u_h^{m+1}(\hat{\epsilon}, \mathbf{k}), \dots, u_h^{m+b_k}(\hat{\epsilon}, \mathbf{k})]$.
- 4: Generate the approximating vectors $\nu_1, \nu_2, \dots, \nu_{N_\nu}$.
- 5: Calculate the matrices $\Psi_{i,j}^1(\mathbf{k})$, and $\Psi_{i,j}^2(\mathbf{k})$.
- 6: Form the linear programming (M_2) and solve this problem for an optimal solution \mathbf{z}^* by interior point method.
- 7: If $\|\mathbf{z}^* - \hat{\mathbf{z}}\| \leq \epsilon_{tol}$, stop and return the optimal solution \mathbf{z}^* . Else update $\hat{\mathbf{z}} = \mathbf{z}^*$ and go to Step 2.

5 Numerical simulation

To verify the quality of our proposed algorithm, it is used to optimize several PBGs of GaAs-based PhCs respectively in this section. For the two common lattices of photonic crystal: square lattice and hexagonal lattice, corresponding numerical experiments are done. The optimized gaps are obviously wider compared with the initial value. We also demonstrate the 3×3 arrays of the unit lattice for the optimized structures of PhCs.

5.1 GaAs-based PhC with square lattice

We first consider two-dimensional GaAs-based PhCs confined to the computational domain of a unit cell of the square lattice. $\mathbf{a} = \Lambda \mathbf{e}_x$ and $\mathbf{b} = \Lambda \mathbf{e}_y$ with lattice constant Λ . The dielectric function ϵ is composed of two materials with dielectric constants $\epsilon_{\min} = 1$ (air) and $\epsilon_{\max} = 11.4$ (GaAs), and the radius $r/\Lambda = 0.375$. The mesh size is $\frac{1}{32}$, and we take $n_k = 60$, $N_\nu = 40$. Band diagrams plotted in the figures below show the eigenvalues moving along the boundary of \mathcal{B} , from X to K to M and back to X as shown in Fig. 3.

Fig. 1 shows the initial PhC structure and its band structure in Section 2. Our proposed algorithm is used to maximize the m -th gap with $m = 2, 4$ and 7 . Fig. 5(a), Fig. 6(a) and Fig. 7(a) show the final optimized band structure of photonic crystal for TM polarization when optimizing the m -th gap. Compared with Fig. 1, it is obvious that the optimized gaps have been significantly improved. Even when there was no band gap before, the band structure with wide-band-gap can be gotten. Fig. 5(b), Fig. 6(b) and Fig. 7(b) show the corresponding optimized structures. The light color indicates the low dielectric constant and the dark color denotes the high dielectric constant. As can be seen from the optimized band structure figures, the width of optimized gap increases signif-

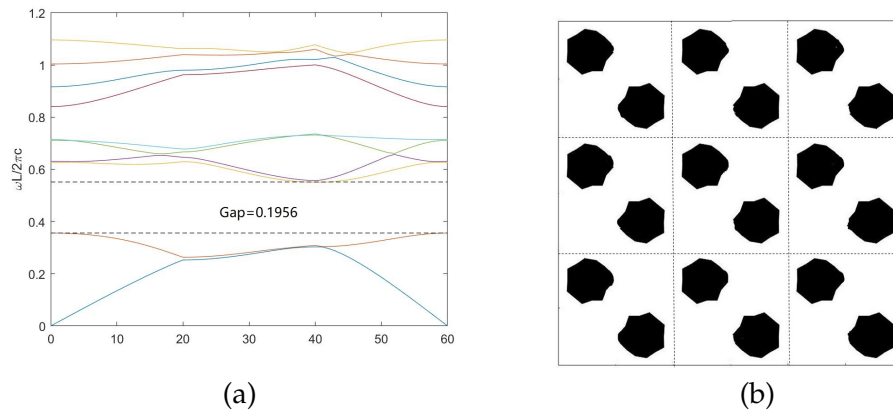


Figure 5: The band structure (a) and the crystal structure (b) for optimizing the second band gap.

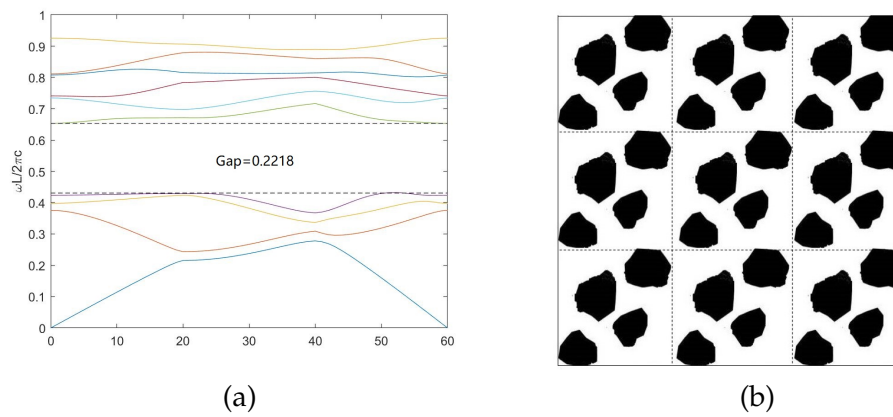


Figure 6: The band structure (a) and the crystal structure (b) for optimizing the fourth band gap.

icantly, which means that the controllable frequency waves are increases. Furthermore, we find that the optimized band gaps are exhibited in isolated high- ϵ structures. This observation has also been pointed out in [17] “the TM bandgaps are favored in a lattice of isolated high- ϵ regions” and observed in [19] previously.

Fig. 8 shows the relationship between the photonic band gap and the iterative step, which also verifies the convergence of our proposed algorithm. From this figure, we can see that the gap is convergent with the increase in the iteration step.

Table 1 shows the average time for each iteration, the initial m -th gap, and the optimized gap to solve the LP problem when optimizing the m -th gap. We note that the gaps mentioned in this paper are the results of normalization. The average times required for each iteration of LP problem are faster than that of SDP, although the optimized gaps of LP are lower than those of SDP. This phenomenon is caused by the finite number of approximate vectors in the simulation. According to Theorem 4.1, we have that the matrix

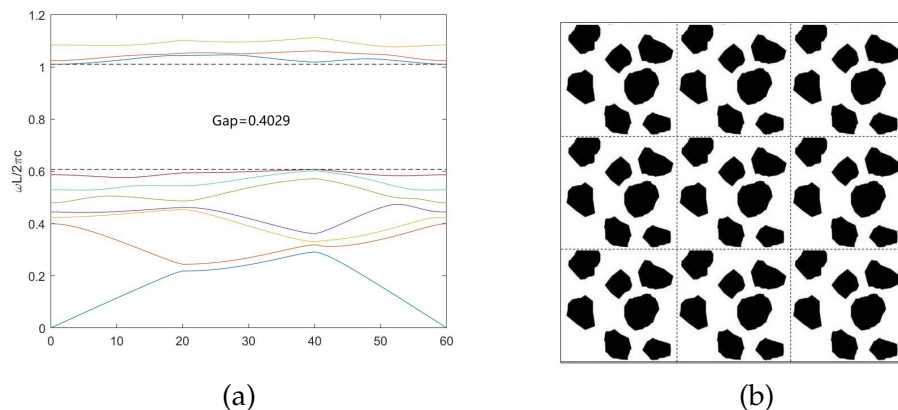


Figure 7: The band structure (a) and the crystal structure (b) for optimizing the seventh band gap.

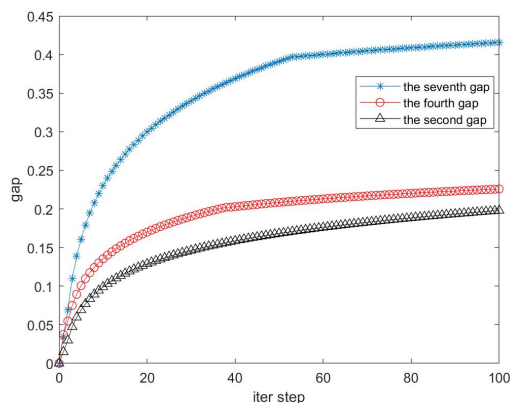


Figure 8: The relationship between the photonic band gap and the iterative step of square lattice.

Ψ is positive semidefinite when $v_k^T \Psi v_k \geq 0, (k=1,2,3,\dots)$. However, in the simulation, the number of approximate vectors can only be limited. The decrease in the degree of freedom affects the final calculation result to a certain extent, that is, the optimized bandgap is a little reduced. In fact, considering a balance between computing time and accuracy, such a result is permissible. In engineering applications, we often do not need particularly high-precision of bandgap, but rather focus on saving calculation time. Reducing calculation time and cost is the focus of engineering [17,31].

5.2 GaAs-based PhC with hexagonal lattice

We also investigate two-dimensional PhCs confined to the computational domain of a unit cell of the hexagonal lattice and present the optimization results for the design of photonic crystals made up of two materials: air and GaAs. $\mathbf{a} = \Lambda \mathbf{e}_x$ and $\mathbf{b} = -\frac{\Lambda}{2} \mathbf{e}_x + \frac{\sqrt{3}\Lambda}{2} \mathbf{e}_y$

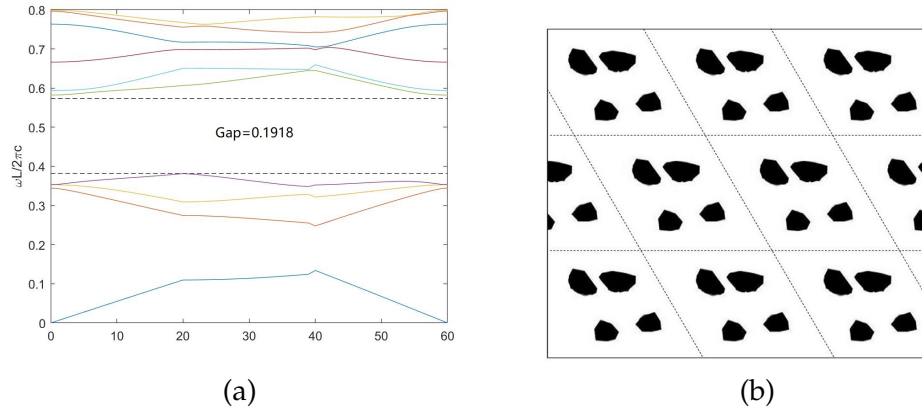


Figure 9: The band structure (a) and the crystal structure (b) for optimizing the fourth band gap.

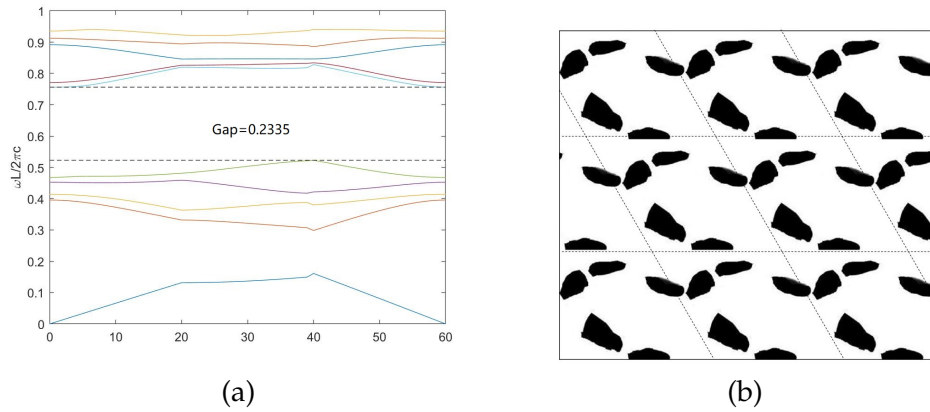


Figure 10: The band structure (a) and the crystal structure (b) for optimizing the fifth band gap.

with the radius $r = 0.375\Lambda$. Also the dielectric function ϵ is composed of two materials with dielectric constants $\epsilon_{\min} = 1$ (air) and $\epsilon_{\max} = 11.4$ (GaAs). The mesh size is $\frac{1}{20}$, and we take $n_k = 60$, $N_v = 40$.

Fig. 2 shows the initial PhC structure with hexagonal lattice and its band structure in Section 2. We use our proposed algorithm to optimize the m -th gap for TM polarization with $m = 4, 5$ and 7 . From Fig. 2, it is clear that the initial gaps all are 0 when $m = 4, 5$

Table 1: Numerical results for the PhC with square lattice.

m	2	4	7
average time (s)	5.97	6.08	6.11
initial gap	0	0	0
optimized gap	0.1956	0.2218	0.4029

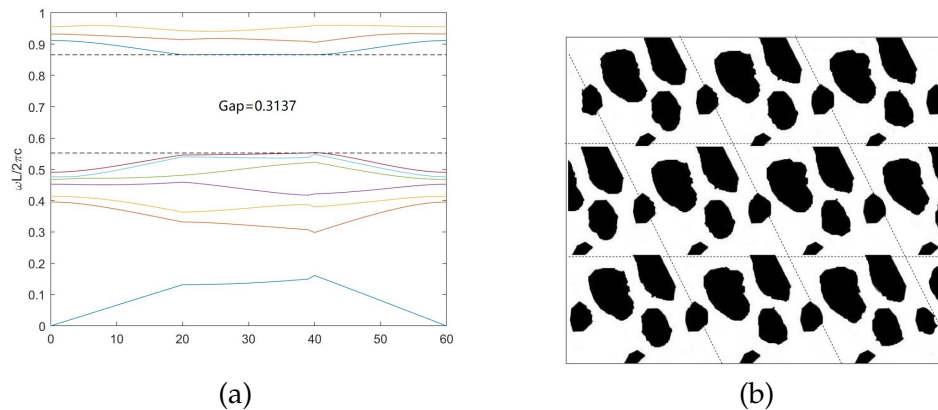


Figure 11: The band structure (a) and the crystal structure (b) for optimizing the seventh band gap.

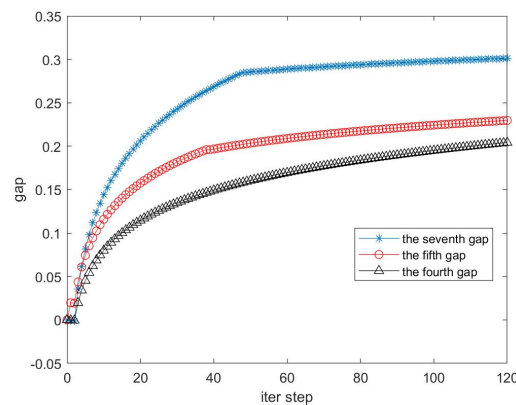


Figure 12: The relationship between the photonic band gap and the iterative step of hexagonal lattice.

and 7. The final optimized band structures of photonic crystal are shown in Fig. 9(a), Fig. 10(a) and Fig. 11(a), respectively. Compared with the initial gap, it is obvious that the optimized gaps have been significantly improved. Fig. 9(b), Fig. 10(b) and Fig. 11(b) show the corresponding optimized structures of photonic crystal, which provide references for the fabrication of PhCs. Also, the dark color denotes the high dielectric constant and the light color indicates the low dielectric constant. The optimized band gaps are also exhibited in isolated high- ϵ structures, just like in the previous summary. Fig. 12 shows the relationship between the photonic band gap and the iterative step. From this figure, it is clear that our proposed algorithm is convergent.

Table 2 summarizes the average time for each iteration, the initial m -th gap, and optimized gap to solve the LP problem when optimizing the m -th gap. The optimized gaps of hexagonal lattice are less than the gaps of square lattice because the degree of freedom of hexagonal lattice finite element discretization is greater. Due to the limited computer

Table 2: Numerical results for the PhC with hexagonal lattice.

m	4	5	7
average time (s)	5.21	5.35	5.77
initial gap	0	0	0
optimized gap	0.1918	0.2335	0.3137

memory, we can only reduce the subdivision accuracy which affects the optimized gaps. In order to ensure the accuracy of the simulations, we discuss possible ways to reduce the computation cost, while optimizing the structures of photonic crystals. On the one hand, there is a potentially large saving when using mesh adaptivity and incorporating a non-uniform grid for the representation of the dielectric function, as well as the eigenvalue calculation [24]. On the other hand, parallel algorithms provide a possibility to solve this problem.

6 Conclusions

In this paper, we propose a convex algorithm to solve the non-convex PDE constrained optimization problems, which is used to design the maximizing the PBGs structure as an application. For our discretize-then-optimize approach, a FEM is first used to discretize the PDE constrained optimization problem. A subspace method is used to reduce the scale of the discrete problem, which can improve the computational efficiency. The discrete optimization problem can be transformed into a simpler convex LP by introducing several artificial variables and approximating the semidefinite cones by judiciously chosen linear bases, thereby further reducing the difficulty of solving the model. We theoretically prove that the LP relaxation problem can approximate the linear SDP problem. And the numerical results also show the effectiveness of this algorithm in maximizing the PBGs of GaAs-based PhC. Furthermore, our algorithm provides a technical route for solving the PDE constrained fractional optimization problems with a generalized eigenvalue constraint and can be easily extended to efficiently solve the PBGs optimization problem of three-dimensional PhCs combined with the three-dimensional finite element techniques.

Acknowledgements

This work was supported by National Natural Science Foundation of China (Grant Nos. 12171052 and 11871115) and BUPT Excellent Ph.D. Students Foundation (Grant No. CX2021320). The authors sincerely thank Prof. Wenbao Ai and Doctor Wei Liang for their valuable discussions. The authors also thank all of the editors and reviewers for their very important suggestions.

References

- [1] G. BAO AND P. LI, *Maxwell's Equations in Periodic Structures*, Springer, 2021.
- [2] G. BAO, Z. XU AND J. YUAN, *Continuation finite element simulation of second harmonic generation in photonic crystals*, *Commun. Comput. Phys.*, 10(2011), pp. 57–69.
- [3] A. BISWAL, R. KUMAR, C. NAYAK AND S. DHANALAKSHMI, *Photonic bandgap characteristics of GaAs/AlAs-based one-dimensional quasi-periodic photonic crystal*, *Optik*, 234 (2021), p. 166597.
- [4] E. CANCES, C. LEBRIS, Y. MADAY, N. NGUYEN, A. PATERA AND G. PAU, *Feasibility and competitiveness of a reduced basis approach for rapid electronic structure calculations in quantum chemistry*, *High-Dimensional Partial Differential Equations in Science and Engineering*, 41(2007), pp. 15–57.
- [5] C. CHEN, R. CHAN, S. MA AND J. YANG, *Inertial proximal ADMM for linearly constrained separable convex optimization*, *SIAM J. Imag. Sci.*, 8 (2015), pp. 2239–2267.
- [6] Y. CHEN AND F. HUANG, *Galerkin Spectral Approximation of Elliptic Optimal Control Problems with H^1 -Norm State Constraint*, *J. Sci. Comput.*, 67 (2016), pp. 65–83.
- [7] S. CHUN AND J. HESTHAVEN, *PDE constrained optimization and design of frozen mode crystals*, *Commun. Comput. Phys.*, 3 (2008), pp. 878–898.
- [8] J.C.DE LOS REYES, *Numerical PDE-Constrained Optimization*, Cham, 2015.
- [9] L. DEKKICHE AND R. NAOUM, *A novel all-optical switch based on a photonic crystal coupler*, *J. Appl. Sci.*, 7 (2007), pp. 3518–3523.
- [10] Y. DUMEIGE, P. VIDAKOVIC, S. SAUVAGE, I. SAGNES, J. LEVENSON, C. SIBILIA, M. CENTINI, G. DAGUANNO AND M. SCALORA, *Enhancement of second-harmonic generation in a one-dimensional semiconductor photonic band gap*, *Appl. Phys. Lett.*, 78 (2001), pp. 3021–3023.
- [11] M. FISHER, J. NOCEDAL, Y. TRÉMOLET AND S.J WRIGHT, *Data assimilation in weather forecasting: a case study in PDE-constrained optimization*, *Optim. Eng.*, 10 (2009), pp. 409–426.
- [12] L. GE, H. NIU, AND J. ZHOU, *Convergence analysis and error estimate for distributed optimal control problems governed by stokes equations with velocity-constraint*, *Adv. Appl. Math. Mech.*, 14 (2020), pp. 33–55.
- [13] K. HSU, W. HUNG, C. CHANG, W. LIN, M. SHIH, P. LEE, S. LIN, S.CHANG, AND Y. CHANG, *Lasing action and extraordinary reduction in long radiative lifetime of type-II GaSb/GaAs quantum dots using circular photonic crystal nanocavity*, *Appl. Phys. Lett.*, 107 (2015), p. 091113.
- [14] Z. HU AND Y. LU, *Propagating bound states in the continuum at the surface of a photonic crystal*, *Journal of the Optical Society of America B*, 34 (2017), pp. 1878–1883.
- [15] X. JIANG, P. LI, J. LV, Z. WANG, H. WU AND W. ZHENG, *An adaptive finite element DtN method for Maxwell's equations in biperiodic structures*, *IMA J. Numer. Anal.*, (2021).
- [16] X. JIANG, L. ZHANG AND W. ZHENG, *On hp-adaptive finite element methods for time-harmonic Maxwell's equations*, *Commun. Comput. Phys.*, 13 (2013), pp. 559–582.
- [17] J. JOANNOPOULOS, R. MEADE AND J. WINN, *Photonic Crystals: Molding the Flow of Light*, Princeton University Press, 2008.
- [18] A. LAPIN, S. ZHANG, S. LAPIN AND N. YAN, *Analysis of finite difference approximations of an optimal control problem in economics*, *Adv. Appl. Math. Mech*, 11 (2019), pp. 1358–1375.
- [19] C. KAO, S. OSHER AND E. YABLONOVITCH, *Maximizing band gaps in two-dimensional photonic crystals by using level set methods*, *Appl. Phys. B Lasers Optics*, 81 (2005), pp. 235–244.
- [20] N. KARMAKAR AND M. MOLLAH, *Potential applications of PBG engineered structures in microwave engineering: Part I*, *Microwave J.*, 47 (2008), pp. 22–44.
- [21] J. LIU, H. GUO AND T. WANG, *A review of acoustic metamaterials and phononic crystals*, *Crystals*, 10 (2020), p. 305.

- [22] Z. LUO, *Theoretical Basis and Application of Finite Element Mixed Method—Development and Application*, Crystals, Shandong Education Press, 1996.
- [23] G. MANZACCA, D. PACIOTTI, A. MARCHESE, M. MOREOLO AND G. CINCOTTI, *2D photonic crystal cavity-based WDM multiplexer*, *Photonics and Nanostructures-Fundamentals and Applications*, 5 (2007), pp. 164–170.
- [24] H. MEN, N. NGUYEN, R. FREUND, P. PARRILO AND J. PERAIRE, *Bandgap optimization of two-dimensional photonic crystals using semidefinite programming and subspace methods*, *J. Comput. Phys.*, (2010), pp. 223–248.
- [25] H. MEN, R. FREUND, N. NGUYEN, J. SAA-SEOANE AND J. PERAIRE, *Designing phononic crystals with convex optimization*, *ASME International Mechanical Engineering Congress and Exposition*, (2013), p. V014T15A047.
- [26] G. PAU, *Reduced-basis method for band structure calculations*, *Phys. Rev. E*, 76 (2007), p. 046704.
- [27] R. PYTLAK, *Conjugate Gradient Algorithms in Nonconvex Optimization*, Springer Science & Business Media, 2008.
- [28] Z. QIAO, T. TANG AND H. XIE, *Error analysis of a mixed finite element method for the molecular beam epitaxy model*, *SIAM J. Numer. Anal.*, 53 (2015), pp. 184–205.
- [29] O. SIGMUND AND K. HOUGAARD, *Geometric properties of optimal photonic crystals*, *Phys. Rev. Lett.*, 100 (2008), p. 153904.
- [30] O. SIGMUND AND J. JENSEN, *Systematic design of phononic band-gap materials and structures by topology optimization*, *Phys. Eng. Sci.*, (2003), pp. 1001–1019.
- [31] CM. SOUKOULIS, *Photonic band Gap Materials*, Springer Science & Business Media, 2012.
- [32] B. SZABÓ AND I. BABUŠKA, *Finite Element Analysis*, John Wiley & Sons, 1991.
- [33] J. WANG AND Y. XIA, *A linear-time algorithm for the trust region subproblem based on hidden convexity*, *Optim. Lett.*, 11 (2017), pp. 1639–1646.
- [34] M. WU, J. YUAN, J. ZHANG, AND W. AI, *Maximizing the photonic band gaps of two-dimensional photonic crystals based on a new subspace method and linear semidefinite programming*, submitted.
- [35] H. XIE, Z. LI AND Z. QIAO, *A finite element method for elasticity interface problems with locally modified triangulations*, *Int. J. Numer. Anal. Model.*, 8 (2011), pp. 189–200.
- [36] K. ZHANG, J. LI, Y. SONG AND X. WANG, *An alternating direction method of multipliers for elliptic equation constrained optimization problem*, *Sci. China Math.*, 60 (2017), pp. 361–378.
- [37] Q. ZHANG, R. ZHANG AND H. SONG, *A finite volume method for pricing the American lookback option*, *T. Acta Physica Sinica*, 64 (2015), p. 070202.
- [38] X. ZHANG AND M. FENG, *A weak galerkin mixed finite element method for acoustic wave equation*, *Adv. Appl. Math. Mech.*, 14 (2022), pp. 936–959.
- [39] Y. ZHOU AND Q. ZOU, *Locally conservative serendipity finite element solutions for elliptic equations*, *Int. Numer. Anal. Model.*, 18 (2021), pp. 19–37.